

# Automated Identification and Measurement of Objects via Populations of Medial Primitives, with Application to Real Time 3D Echocardiography

George D. Stetten<sup>1,2</sup> and Stephen M. Pizer<sup>1</sup>

<sup>1</sup> Medical Image Display and Analysis Group, UNC, Chapel Hill  
george@stetten.com, smp@cs.unc.edu

<sup>2</sup> NSF/ERC for Emerging Cardiovascular Technologies, Duke University

**Abstract.** We suggest that identification and measurement of objects in 3D images can be automatic, rapid and stable, based on the statistical properties of populations of medial primitives sought throughout the image space. These properties include scale, orientation, endness, and medial dimensionality. The property of medial dimensionality differentiates the sphere, the cylinder, and the slab, with intermediate dimensionality also possible. Endness results at the cap of a cylinder or the edge of a slab. The values of these medial properties at just a few locations provide an intuitive and robust model for complex shape. For example, the left ventricle during systole can be described as a large cylinder with an apical cap at one end, a slab-like mitral valve at the other (closed during systole), and appropriate interrelations among components in terms of their scale, orientation, and location. We demonstrate our method on simple geometric test objects, and show it capable of automatically identifying the left ventricle and measuring its volume *in vivo* using Real-Time 3D echocardiography.

## 1 Introduction

The lineage of the medial approach may be traced to the medial axis (otherwise known as symmetric axis or skeleton) introduced on binary images by Blum and developed by Nagel, Nackman, and others [1–3]. Pizer has extended the medial axis to gray-scale images producing a graded measure called *medialness*, which links the aperture of the boundary measurement to the radius of the medial axis to produce what has been labeled a *core*, a locus in a space of position, radius, and associated orientations [4, 5]. Methods involving these continuous loci of medial primitives have proven particularly robust against noise and variation in target shape [6]. Determining locations with high medialness and relating them to a core has been accomplished by analyzing the geometry of loci resulting from ridge extraction [7]. Models including discrete loci of medial primitives have also provided the framework for a class of active shape models known as *Deformable Shape Loci* [8].

The objective of the work reported here is to build on these ideas to produce a method for analyzing the shape of the heart in Real Time 3D ultrasound, a new imaging modality that uses a matrix array of transducer elements to scan the moving heart in 3D at more than 20 frames/second [9]. The approach to analyzing this data aims to extract the scale, orientation and dimensionality (shape type) of sections of cardiac anatomy by statistical analysis of populations of medial primitives. In particular, the primitives are identified by first searching for individual boundary points throughout the image in an initial sweep, and then by matching pairs of boundary points to form what are called *core atoms*. Core atoms tend to cluster along a medial ridge and allow for statistical analysis of the core and its underlying figure. Core atoms have already been developed for analysis of 2D shape [10] and are generalized here to 3D. The analysis is also extended to spatially sampled populations of core atoms. This research is part of a Ph.D. dissertation which covers many aspects in greater detail [11].

## 2 What is a Core Atom?

A *core atom* is defined as two boundary points  $\mathbf{b}_1$  and  $\mathbf{b}_2$  that satisfy particular requirements (described in detail below) guaranteeing that the boundaries face each other. A core atom can be represented by a single vector  $\mathbf{c}_{1,2}$  from the first boundary point to the second. The core atom is said to be “located” at a *center point* midway between the boundary points (see Fig. 1). The *medialness* at the center point is high because the *boundariness* at both boundary points is high and because the boundary normals face each other. Core atoms carry orientation, width and position, providing the ability for populations of core atoms to be analyzed in these terms.

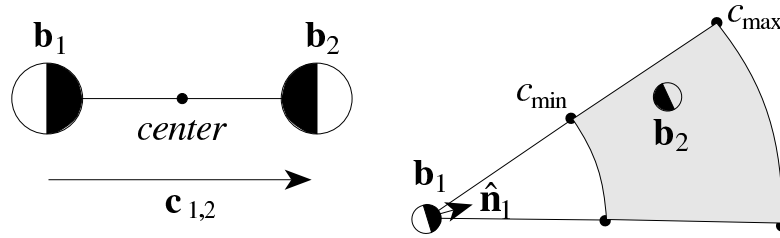


**Fig. 1.** A core atom consists of two boundary points that face each other across an acceptable distance, and a center point at which the core atom is said to be located. The search area (gray) for boundary point  $\mathbf{b}_2$  determined by boundary normal  $\hat{\mathbf{n}}_1$

Unlike medial models where *object angle* (half the angle between lines from the center point to each respective boundary point) is permitted to vary, the object angle of a core atom is fixed at  $90^\circ$ . Core atoms thus follow in the tradition of Brady [12]. As in Brady, the underlying figure is not required to have

parallel boundaries. In the experiments presented below, boundariness is based on a Difference of Gaussian (DOG) measurement of intensity gradient, accomplished by repeated application of a binomial kernel. The number of applications determines the aperture of the boundariness detector, and is generally proportional to the size of the core atom. Further constraints are placed on the levels of intensity along the gradient direction. Other forms of boundariness, such as those based on texture analysis, could also be used for core atoms, provided an orientation is established for each boundary point.

Boundariness vectors are sampled on a rectilinear grid, and their magnitude compared to a threshold to select a population of boundary points  $\mathbf{b}_i$  at locations  $\mathbf{x}_i$  with orientations  $\hat{\mathbf{n}}_i$  (“ $\hat{\mathbf{v}}$ ” denotes normalization,  $\hat{\mathbf{v}} \equiv \mathbf{v}/\|\mathbf{v}\|$ ). The strength inherent to the statistics of populations is meant to counteract the weakness of thresholding. Core atoms are created from this population by finding pairs of candidate boundary points that satisfy the following three criteria:

1. The magnitude of the core atom vector  $\mathbf{c}_{1,2}$ , i.e., the distance from one boundary point to the other, must be between  $c_{min}$  and  $c_{max}$ .

$$\mathbf{c}_{1,2} = \mathbf{x}_2 - \mathbf{x}_1 \quad c_{min} \leq \|\mathbf{c}_{1,2}\| < c_{max}. \quad (1)$$

The core atom vector can be oriented either way since the order of the boundary points is arbitrary.

2. The boundary points must have sufficient face-to-faceness defined as

$$F(\mathbf{b}_1, \mathbf{b}_2) = f_1 \cdot f_2 \quad f_1 = \hat{\mathbf{c}}_{1,2} \cdot \hat{\mathbf{n}}_1 \quad f_2 = \hat{\mathbf{c}}_{2,1} \cdot \hat{\mathbf{n}}_2. \quad (2)$$

Since  $f_1$  and  $f_2$  are normalized to lie between +1 and -1, their product  $F$  must also lie between +1 and -1. Values for  $F$  near +1 occur when the boundaries face towards (or away from) each other across the distance between them. A threshold for acceptable face-to-faceness is set within some error  $\epsilon_f$  such that  $F(\mathbf{b}_1, \mathbf{b}_2) > 1 - \epsilon_f$ .

3. Assuming  $F(\mathbf{b}_1, \mathbf{b}_2) > 0$ , it follows that  $f_1$  and  $f_2$  are both positive, or both negative. The sign of  $f_1$  (or  $f_2$ ) is called the *polarity*. The appropriate polarity is either + or - depending on whether the expected target is lighter or darker than the background.

Although at first glance the search for pairs of boundary points appears to be  $O(n^2)$ , hashing individual boundary points beforehand by location yields a large reduction in computation time. The search area for  $\mathbf{b}_2$  is limited to a solid sector surrounding the orientation  $\hat{\mathbf{n}}_1$  of the *first* boundary point, and to a range between  $c_{min}$  and  $c_{max}$ . The width of the sector depends on  $\epsilon_f$  (see Fig. 1).

### 3 Three Basic Configurations: Sphere, Cylinder, and Slab

Observe that collections of core atoms can group in three basic ways corresponding to the fundamental geometric shapes shown Fig. 2. The surfaces are shown

in dark gray with the corresponding cores shown in light gray. Beneath each object is the population of core atoms that would be expected to form with such objects, the core atoms being depicted as simple line segments.

The sphere generates a “Koosh ball” like cloud of core atoms with spherical symmetry, with the core atom centers clustered at the center of the sphere. The cylinder generates a “spokes-of-a-wheel” arrangement with radial symmetry along the axis of the cylinder, and the core atom centers clustered along the axis of the cylinder. The slab results in a “bed-of-nails” configuration across the slab, with core atom centers clustered in the mid-plane of the slab. It is reassuring to find that the cores of these basic objects are the point, the line, and the plane. As shown in Fig. 2, a system of shape-specific coordinate axes, namely  $\hat{\mathbf{a}}_1$ ,  $\hat{\mathbf{a}}_2$ , and  $\hat{\mathbf{a}}_3$ , can be assigned in each case, although not all the axes are unique given the symmetries involved. For example, in the slab,  $\hat{\mathbf{a}}_1$  and  $\hat{\mathbf{a}}_2$  can rotate freely about  $\hat{\mathbf{a}}_3$ . Such a set of coordinate axes can be found for any population of core atoms using eigenanalysis, as will be shown below. Furthermore, the extent to which a core atom population resembles one of the three basic configurations depends on the corresponding eigenvalues.

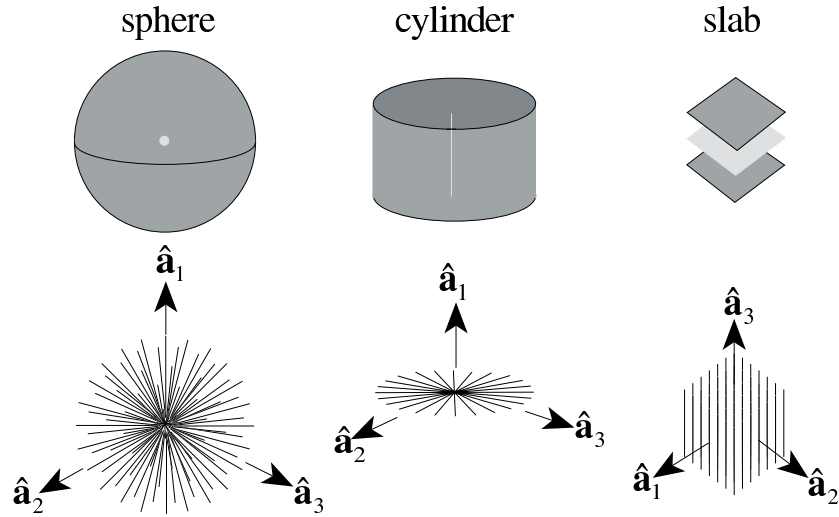


**Fig. 2.** Fundamental shapes (dark gray), corresponding cores (light gray), core atom populations (line segments) and eigenvectors  $\hat{\mathbf{a}}_1$ ,  $\hat{\mathbf{a}}_2$  and  $\hat{\mathbf{a}}_3$

Given a population of  $m$  core atoms  $\mathbf{c}_i$ ,  $i = 1, 2, 3, \dots, m$ , the analysis of a core atom population begins by separating each core atom vector  $\mathbf{c}_i$  into its magnitude  $c_i$  and its orientation  $\hat{\mathbf{c}}_i$ . We ignore, for the moment, the location of the core atom. The analysis of magnitude  $c_i$  over a population of core atoms is straightforward, yielding a mean and standard deviation for the measurement of width in the underlying figure. The orientation  $\hat{\mathbf{c}}_i$  of core atoms in a population lends itself

to eigenanalysis, yielding measures of dimensionality and overall orientation for the population. We develop the eigenanalysis here in  $n$  dimensions, although for the remainder of the paper  $n$  will be 3.

Given the population of  $m$  vectors in  $n$  dimensions, we find an  $n$ -dimensional vector  $\hat{\mathbf{a}}_1$  that is most orthogonal to that population as a whole by minimizing the sum of squares of the dot product between  $\hat{\mathbf{a}}$  and each individual  $\hat{\mathbf{c}}_i$ .

$$\hat{\mathbf{a}}_1 = \arg \min_{\hat{\mathbf{a}}} \frac{1}{m} \sum_{i=1}^m (\hat{\mathbf{a}} \cdot \hat{\mathbf{c}}_i)^2 = \arg \min_{\hat{\mathbf{a}}} (\hat{\mathbf{a}}^T C \hat{\mathbf{a}}) \quad \text{where } C = \frac{1}{m} \sum_{i=1}^m \hat{\mathbf{c}}_i \hat{\mathbf{c}}_i^T. \quad (3)$$

The  $C$  matrix is positive definite, symmetric, and has a unit trace. Therefore, its eigenvalues are positive and sum to 1, and its eigenvectors are orthogonal. If the eigenvalues of  $C$  are sorted  $\lambda_1 \leq \lambda_2 \leq \dots \leq \lambda_n$ , the corresponding eigenvectors  $\hat{\mathbf{a}}_1 \dots \hat{\mathbf{a}}_n$  are the axes of a coordinate system in which  $\hat{\mathbf{a}}_1$  is the most orthogonal to the population  $\hat{\mathbf{c}}_i$  as a whole. For example, it would be the axis of the cylinder in Fig. 2. Furthermore, the eigenanalysis guarantees that  $\hat{\mathbf{a}}_2$  is the most orthogonal to the population  $\hat{\mathbf{c}}_i$  among those directions that are already orthogonal to  $\hat{\mathbf{a}}_1$ . This process can be repeated until  $\hat{\mathbf{a}}_n$  remains the *least* orthogonal to the population  $\hat{\mathbf{c}}_i$ , representing a form of *average* orientation for  $\hat{\mathbf{c}}_i$ .

## 4 The Lambda Triangle

Returning now specifically to 3D, the previous analysis yields three eigenvalues which describe the dimensionality of the core.

$$\lambda_i \geq 0 \quad \lambda_1 + \lambda_2 + \lambda_3 = 1. \quad (4)$$

An eigenvalue of zero means that the corresponding eigenvector is perfectly orthogonal to every core atom  $\hat{\mathbf{c}}_i$ . Such is the case for  $\hat{\mathbf{a}}_1$  in the cylinder, and for both  $\hat{\mathbf{a}}_1$  and  $\hat{\mathbf{a}}_2$  in the slab. In the sphere none of the eigenvectors is completely orthogonal to the core atom population. Given the symmetries of the three basic shapes, the eigenvalues shown in Fig. 3 result.

Since  $\lambda_3$  is dependent on the other two, the system may be viewed as having only two independent variables,  $\lambda_1$  and  $\lambda_2$ . Because of constraints already mentioned, possible values for  $\lambda_1$  and  $\lambda_2$  are limited by  $\lambda_1 \leq \lambda_2$  and  $\lambda_2 \leq (1 - \lambda_1)/2$  which define a triangular domain we call the *lambda triangle* (Fig. 3).

The vertices of the lambda triangle correspond to the three basic shapes in Fig. 2, with all possible eigenvalues falling within the triangle. A rather crude simplification of dimensionality is possible by dividing the triangle into three compartments to provide an integer description of dimensionality. Arbitrary thresholds of  $\lambda_1 = 0.2$  and  $\lambda_2 = 1/3$  will be used to divide the triangle into such areas of integer dimensionality to clarify our experimental results. However, it should be remembered that the underlying dimensionality is not an integer or even a single scalar, but rather two independent scalars,  $\lambda_1$  and  $\lambda_2$  whose values are constrained by the lambda triangle.

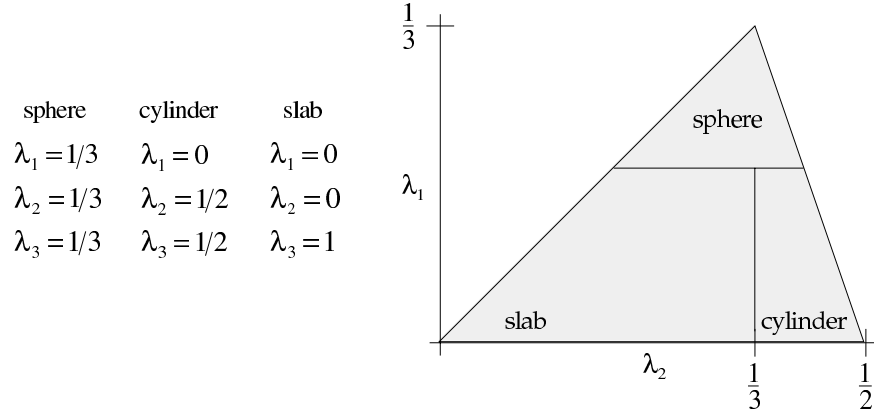


**Fig. 3.** The lambda triangle defines the domain of possible eigenvalues

## 5 Spatial Sampling in the Corona

We now return to the question of core atom location, which we have so far ignored. To incorporate location into the analysis of core atoms, we sort them into bins on a regular 3D lattice by the location of their center points. Thus each bin represents a spatial sampling of medialness. The number of core atoms in a sample volume can be thought of as the *medial density* at that location.

How do we choose an appropriate size for the sample volume? As we shall see, the local distribution of core atoms can have a significant cross section, and the density within that distribution may not be uniform. To preserve resolution, the sample volume needs to be smaller than the typical cross section of a core atom cloud. When a core is sampled off-center, it will demonstrate a distortion in its dimensionality. For example, the zero-dimensional core at the center of a sphere will appear to be one-dimensional (cylindrical) when sampled off center, as shown in Fig. 4. The vector from the theoretical core (center of the sphere) to the center of the density in the sample volume is called the *displacement vector*  $\mathbf{p}$  (See Fig. 4C). The core atom population within a sample volume may not contain the entire thickness of the core, but rather a sub-sampling of the core called a *coronal density*. We can generally expect, in fact, to be sampling coronal densities. It would be helpful to know where, in a given cloud around the core, a sample was collected, but that presupposes knowledge about the overall distribution of core atoms which we may not have.

We can, at least, predict certain relationships to exist between the distribution of core atoms over the entire core and that of a sample volume displaced from the center of the core. The displaced sample of core atoms will be flattened in a plane orthogonal to  $\mathbf{p}$ , and thus develop orthogonality to that direction. This can be seen in Fig. 4, where the spherical distribution of core atoms in 4B has been flattened into a cylindrical distribution in 4C. The same effect can be seen

in the case of the cylinder in Fig. 5, where, displaced off the central axis of the cylinder by  $\mathbf{p}$ , the population of core atoms becomes slab-like and orthogonal to  $\mathbf{p}$ . One expects the displacement vector to be one of the eigenvectors at the closest point on the theoretical core, because (1) the displacement vector will be orthogonal to the core at that point, and (2) the normal to the core is always one of its eigenvectors. In 3D, the medial manifold can have at most 2 dimensions and thus will always have such a normal.

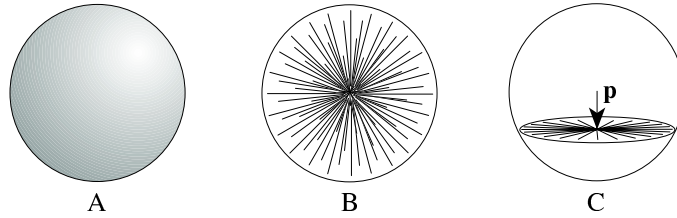


Fig. 4. A. sphere. B. all core atoms C. cylindrical coronal density displaced by  $\mathbf{p}$

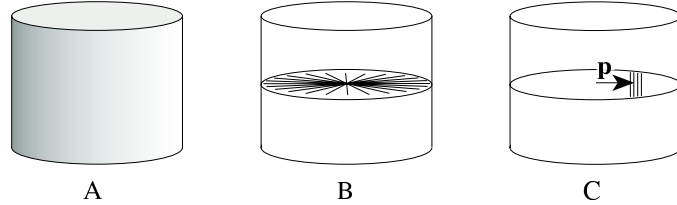
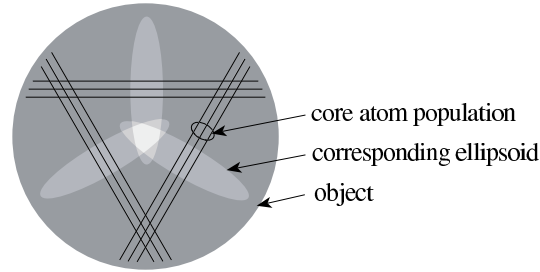


Fig. 5. A. cylinder. B. all core atoms C. slab-like coronal density displaced by  $\mathbf{p}$

Figs. 4 and 5 suggest that the displacement vector  $\mathbf{p}$  could somehow be used to compensate for the dimensional distortion in the corona. However, an isolated density that is, for example, cylindrical cannot know whether it represents the true center of a cylinder or simply the corona of a sphere. The results of the eigenanalysis for each density may be used in a Hough-like fashion simultaneously to vote for its own dimensionality and center of mass, and for possible densities whose corona it may inhabit. The voting takes place within ellipsoids around each density. The axes of each ellipsoid are long in directions orthogonal to the core atom population in its density. Thus the ellipsoid can be expected to extend in the  $\mathbf{p}$  direction, orthogonal to the core atoms.

Fig. 6 demonstrates this concept. A circular cross-section through an object is shown with three coronal densities (each containing 3 core atoms) displaced from the center. An ellipsoid is associated with each density, with the major axis of each ellipsoid along the eigenvector most orthogonal to the corresponding



**Fig. 6.** Ellipsoids of three coronal core atom densities coalescing at the true center

core atoms. The three ellipsoids intersect at the center the circle. The figure can be interpreted as the cross-section of a sphere with the populations of core atoms being cylindrical (seen in cross-section) and the ellipsoids intersecting at the center of the sphere (as in Fig. 4). Alternatively it can be interpreted as the cross-section of a cylinder with the populations of core atoms being slab-like and the ellipsoids intersecting along the axis of the cylinder (as in Fig. 5). There are various ways to construct such ellipsoids. We have chosen the following heuristic for its simplicity. The axes of each ellipsoid are the eigenvectors of its density's  $C$  matrix. The lengths  $a_i$  of the axes are related to the eigenvalues  $\lambda_i$  as follows:

$$a_1 = \gamma\bar{c}, \quad a_2 = \frac{\alpha_2}{\alpha_1}a_1, \quad a_3 = \frac{\alpha_3}{\alpha_1}a_1 \quad \text{where } \alpha_i = 1 - \lambda_i, \quad \gamma = \frac{1}{2}. \quad (5)$$

The scalar distance  $\bar{c}$  is the mean diameter of the core atoms in the density, and the dimensionless number  $\gamma$  relates  $\bar{c}$  to the size of the ellipsoid, determining how many neighbors will be reached. The ellipsoids make it possible to cluster the core atoms for a given cloud, in effect to coalesce the corona. Each sample volume (the *votee*) receives votes from all the neighboring sample volumes whose ellipsoids overlap it. The votes from those ellipsoids are assigned a strength  $v$ , where  $v = m \cdot \exp(-d_e^2)$ ,  $m$  being the number of core atoms in the voting density, and  $d_e$  the ellipsoidal distance

$$d_e = \sqrt{\sum_{i=1}^3 \left( \frac{\hat{\mathbf{a}}_i \cdot \mathbf{d}}{a_i} \right)^2}. \quad (6)$$

from the center of the voter ellipsoid to the votee,  $\mathbf{d}$  being the vector from the voter to the votee. Votes are constructed to contain information about the voter, including its  $C$  matrix which may simply be summed (scaled by  $v$ ) for an eigenanalysis of the entire constituent core atom population of a particular candidate. Thus are formed what we call *superdensities*, clusters of core atoms that no longer suffer from coronal distortion. The center of mass for the constituent core atom population of a superdensity will tend to be at the true core, rather than in the corona.

## 6 Tests with Parametric Objects

To validate these methods, we applied them to three parametric test objects with simple geometries: a sphere, a torus, and a spherical shell. The torus is basically a cylinder of varied and known orientation, and the spherical shell is likewise a slab of varied and known orientation. (The sphere is simply itself.)

Eigenanalysis of the coronal densities collected in a rectilinear lattice of sample volumes yielded the following results. Fig. 7 shows all densities containing greater than 1% of the entire core atom population plotted on the lambda triangle. The sphere shows two groups of densities, one near the top (sphere) vertex of the triangle and another near the right (cylinder) vertex, consistent with the dimensional effects of the corona predicted in Fig. 4. The torus, which is locally a cylinder, shows clustering near the right (cylinder) vertex, with some spreading towards the left (slab) consistent with the dimensional effects of the corona predicted in Fig. 5. The spherical shell, which is locally a slab, shows tight clustering at the left (slab) vertex consistent with the observation that core atoms in a slab are collinear with  $\mathbf{p}$  and therefore will not develop significant orthogonality.

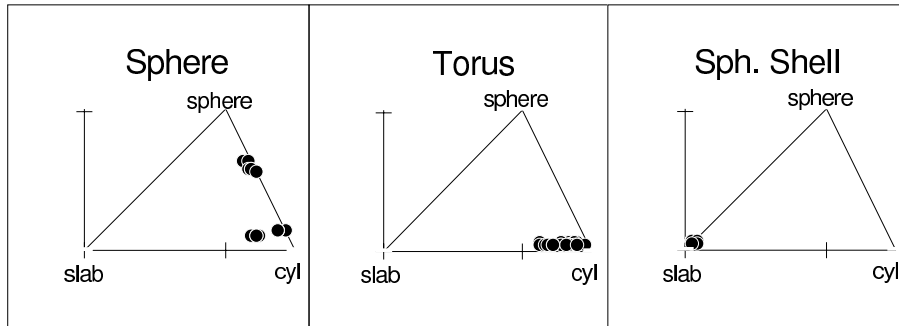


Fig. 7. Distribution of densities on lambda triangles, for parametric test objects

Unfortunately, Fig. 7 does not contain spatial information about the sampled densities. The spatial distribution of densities for the test objects is shown Fig. 8. Each sample volume whose density contains more than 1% of the total core atoms is shown as a thin-lined symbol. The simple partition of the lambda triangle in Fig. 3 is used to decide between three possible symbols: a slab is represented as a single line, a cylinder as a cross, and a sphere as 3 intersecting axes. The length of the thin lines is constant, chosen for clarity in each test object. The orientation of the thin lines indicates the predominant direction(s) of core atoms in each density, i.e. across the slab, or orthogonal to the axis of the cylinder, keeping in mind that perfect spheres have no predominant orientation and perfect cylinders allow arbitrary rotation around the axis.

As expected the sphere shows cylindrical densities in its corona oriented towards the center. Further out from the center a few slabs-like densities reflect

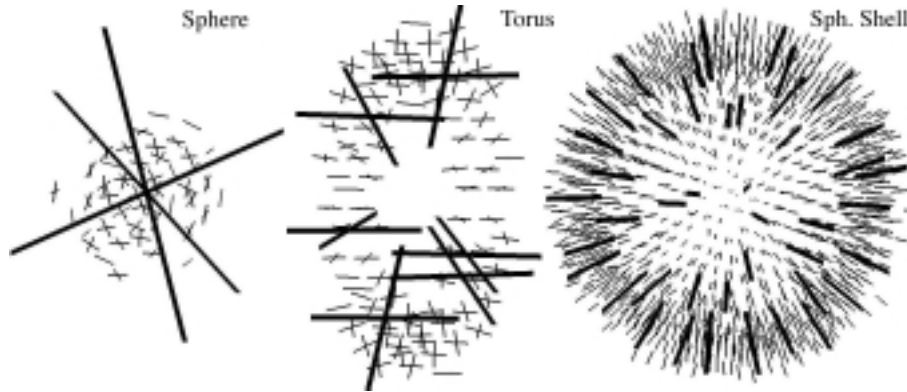


Fig. 8. Densities and superdensities for parametric objects

simply the paucity of core atoms in those sample volumes. Near the center one true spherical density (a small 3-axis symbol) may be discerned. The thick-lined symbols show the results of ellipsoidal voting, i.e., they represent superdensities. To prevent a cluttered illustration, superdensities are limited to non-overlapping constituencies. They are represented by thick lines in a manner similar to the densities, except the length of the axes now corresponds to the actual mean scale of the constituent core atoms. Thus the thick-lined 3-axis cross indicates the actual diameter of the spherical object. For the sphere there is only one predominant winning superdensity, with virtually every core atom in its constituency. The torus shows cylindrical densities properly oriented but dispersed throughout the corona. At the outer regions of the corona a few slab-like densities are visible. The superdensities, by contrast, are centered on the circular mid-line of the torus. The spherical shell shows only slab-like densities, which coalesce with ellipsoidal voting into slab-like superdensities. The orientation of both are across the local slab. Ellipsoidal voting is seen to perform another function, that of connecting densities that share a core along the mid-plane of a slab or the axis of a cylinder.

## 7 Endness

Some attention must be paid to cases where a cylinder ends at a hemispherical cap, or a slab ends at a hemicylindrical edge. The property of endness has been described by Clary, et al. [13]. Endness as viewed from the core atom perspective is illustrated in Fig. 9A and 9B. To detect endness, densities of core atoms are used as starting points. Once a local cylinder has been established, boundary points are sought along the axis of the cylinder in either direction as evidence of a cap. Similarly, once a local slab has been found, boundary points indicating an edge can be sought. Mathematics for this is derived elsewhere [11].

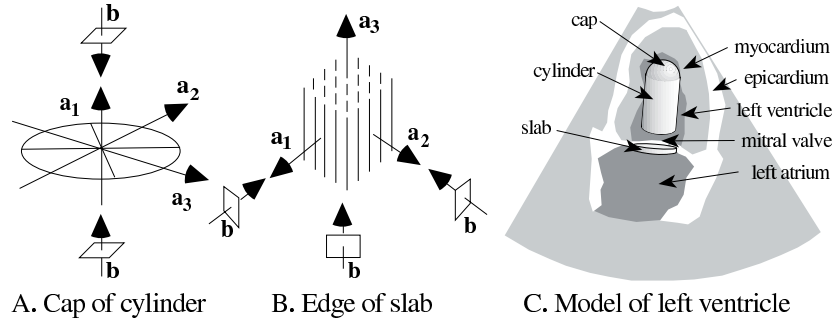


Fig. 9. Endness, manifested as a cap on a cylinder (A) and the edge of a slab (B)

## 8 Identifying and Measuring the Cardiac Left Ventricle

We now turn to a useful clinical application, the automated determination of left ventricular volume using Real Time 3D (RT3D) echocardiography. RT3D is a new imaging modality that electronically scans a volume in 3D using a matrix array instead of the conventional linear array. RT3D is described in detail elsewhere [9], but its primary novelty is the ability to capture a single cardiac cycle at 22 frames/second, which no other available imaging modality can accomplish.

RT3D images of an *in vivo* human heart present a significant challenge to image analysis techniques, including high noise, low resolution, path dependence, and a non-rectilinear data space. These problems are addressed elsewhere [11], but the suggestion that the statistical nature of our method yields robustness is severely tested in its application to RT3D echocardiography.

We now expand on the example from the abstract: The left ventricle during systole is basically a large cylinder with an apical cap at one end, and a slab-like mitral valve at the other (we limit ourselves here to apical scans, and to times when the mitral valve is closed). The model is shown in Fig. 9C. To identify the cylinder in the image data, core atoms of an appropriate range of diameters were collected in sample volumes on a regular lattice, and ellipsoidal voting was applied. An example of the resulting superdensities is displayed in Fig. 10A. Crosses are shown in the cylindrical chamber of the ventricle. Due to the pre-selection of core atoms by scale, no other significant densities of core atoms were found.

Next, the mitral valve was sought, by limiting the formation of core atoms to an appropriately smaller scale, and to orientations nearly perpendicular to the transducer. As shown in Fig. 10B, the strongest superdensities (short vertical line segments) were clustered around the center of the mitral valve, although weaker false targets were detected in the myocardium. To eliminate these false targets, a criterion was established for the formation of appropriate pairs of superdensities, in the spirit of core atoms. Only slab-like densities appropriately located and oriented with respect to cylindrical densities were accepted. These pairs were allowed to vote for their constituent superdensities, and the mean

location of the winning superdensities used to establish a single mitral valve location and a single LV cylinder location. The vector between these two locations was used to establish a cone for expected boundary points at the apex of the LV, and the mean distance to the resulting boundary points used to determine the location of the apical cap along that vector. Thus an axis between the apex and the mitral valve was established. Given this axis, LV volume was estimated by collecting boundary points around the axis. Only boundaries that faced the axis were accepted. The boundary points were organized into bins using cylindrical coordinates, in other words, disks along the axis and sectors within each disk. An average radius from the axis was established for the boundary points in each bin, creating a *surface map* of the endocardial surface. Fig. 10C shows such a surface map (dots) and the underlying axis. The problem of empty bins was avoided by convolving the surface map with a binomial kernel in 2D until each bin had some contribution to its average radius. Volumes were then calculated by summing over all sectors. The entire procedure including identification and volume measurement of the LV was automated, and required approximately 15 seconds on a 200 MHz Silicon Graphics O2 computer.

The automated volumes were compared to manual tracings performed on a stack of flat slices orthogonal to a manually-placed axis (see Fig. 10D). This axis employed the same anatomical end-points (the ventricular apex and the center of the mitral valve) as the axis determined automatically above. The volumes and locations of the end-points were compared to those determined automatically. Results are shown in Fig. 11. They are very encouraging, particularly for the automated placement of the axis end points, which had an RMS error of approximately 1 cm. Volume calculations introduced additional errors of their own, but were still reasonable for ultrasound. Only four cases have been tried, and all are shown. The method worked in all cases.

## 9 Conclusions

We have described a new method for identifying anatomical structures using fundamental properties of shape extracted statistically from populations of medial primitives, and have demonstrated its feasibility by applying it under challenging conditions. Further studies are presently underway to establish reliability over a range of data. Future directions include introducing greater specificity and adaptability in the boundary thresholding, incorporating more than 2 nodes into the model, introducing variability into the model to reflect normal variation and pathologic anatomy, extending the method to the spatio-temporal domain, and applying it to visualization.

## Acknowledgments

Whitaker Biomedical Engineering grant, NSF grant CDR8622201, NIH grants 1K08HL03220, P01CA47982, HL46242, data from Volumetrics, Durham, NC.

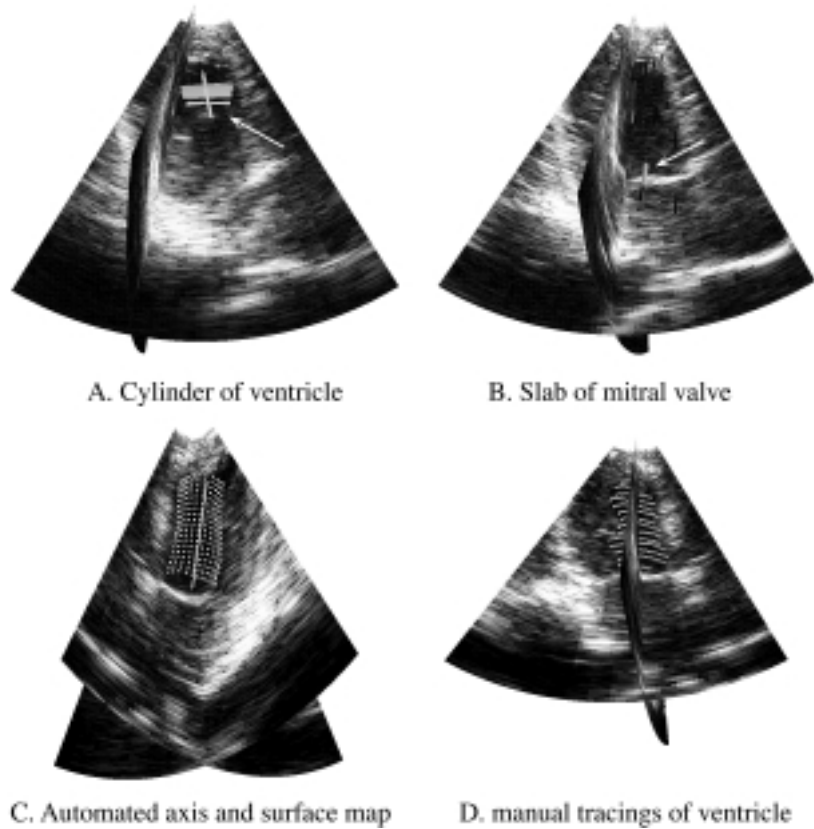


Fig. 10. Real Time 3D ultrasound with automated and manual identification of LV

## References

1. Blum, H and Nagel, R.N.: Shape description using weighted symmetric axis features. *Pattern Recognition* **10** (1978) 167-180
2. Nackman, L.R.: Curvature relations in 3D symmetric axes, *CVGIP* **20** (1982) 43-57
3. Nackman, L.R., and Pizer, S.M.: Three-Dimensional shape description using the symmetric axis transform I:Theory. *IEEE Trans. PAMI* **2** (1985) 187-202
4. Burbeck, C.A., and Pizer, S.M.: Object representation by cores: Identifying and representing primitive spatial regions. *Vision Research* **35** (1995) 1917-1930
5. Pizer, S.M., Eberly, D.H., Morse, B.S., and Fritsch, D.S.: Zoom invariant vision of figural shape: the mathematics of cores. *Computer Vision and Image Understanding* **69** (1998) 55-71
6. Morse, B.S., Pizer, S.M., Puff, D.T., and Gu, C.: Zoom-Invariant vision of figural shape: Effect on cores of image disturbances. *Computer Vision and Image Understanding* **69** (1998) 72-86
7. Furst, J.D., and Pizer, S.M.: Marching Cores: A method for extracting cores from 3D medical images. *Proceedings of the Workshop on Mathematical Methods in Biomedical Image Analysis*, San Francisco, CA, June 1996.

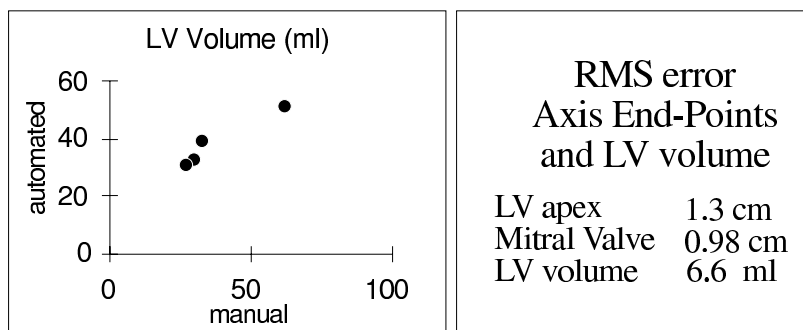


Fig. 11. Volume measurement and axis end-point location, manual vs. automatic

8. Fritsch, D., Pizer, S.M., Yu, L., Johnson, V., and Chaney, E.: Segmentation of Medical Image Objects Using Deformable Shape Loci. Information Processing in Medical Imaging, Poultney, Vermont (1997)
9. Stetten, G., Ota, T., Ohazama, C., Fleishman, C., Castelucci, J., Oxaal, J., Kisslo, J., and Ramm, O.T.v.: Real-Time 3D Ultrasound: A New Look at the Heart. J. Cardiovasc. Diagnosis and Proc. **15** (1998) 73-84
10. Stetten, G., Landesman, R., and Pizer, S.M.: Core-Atoms and the spectra of scale, (Technical Report TR97-006, UNC Dept. Computer Science. SPIE Medical Imaging Conference (1997)
11. Stetten, G.: Automated Identification and Measurement of Cardiac Anatomy Via Analysis of Medial Primitives. Ph.D. Dissertation, Stephen Pizer, advisor, UNC Chapel Hill, (expected, 1999).
12. Brady, M.: Criteria for representations of shape. New York, Academic Press (1983)
13. Clary, G.J., Pizer, S.M., Fritsch, D.S., and Perry, J.R.: Left ventricular wall motion tracking via deformable shape loci. CAR International Symposium and Exhibition, Amsterdam (1997)